Proceedings of the 15th European Conference on Soil Mechanics and Geotechnical Engineering
A. Anagnostopoulos et al. (Eds.)
IOS Press, 2011

doi:10.3233/978-1-60750-801-4-749

Experimentally observed settlements beneath shallow foundations on sand

Des essais pour observer des tassements sous les fondations superficielles sur du sable

B. T. McMahon[1] & M.D. Bolton
Department of Engineering, University of Cambridge

ABSTRACT

Shallow foundations are designed by geotechnical engineers on a daily basis. Settlements are predicted based on elastic properties of soil. Soil is, however, non-linear even at small strains. A method was developed for testing circular shallow foundations on sand in the beam centrifuge at Cambridge University. The problem of bedding errors due to an uneven sand surface had to be overcome. Digital images were captured during the loading of soil bodies to observe deformation mechanisms. Instrumentation was used to confirm various quantities. Mechanisms and strain plots have been presented along with a comparison between settlements observed and a trial prediction based on the concepts of Mobilizable Strength Design (MSD).

RÉSUMÉ

Les fondations superficielles sont conçues par les ingénieurs géotechniques quotidiennement. On prévoit les tassements selon les propriétés du sol. Le sol est, cependant, non-linéaire, même sous de petites contraintes. Une méthode a été développée pour essayer les fondations superficielles circulaires sur du sable, dans la Centrifugeuse Géotechnique à l'Université de Cambridge. On a dû surmonter le problème des surfaces inégales du sable. Des images digitales ont été saisies pendant le chargement du sol, pour observer les mécanismes de déformation. On a employé l'instrumentation pour confirmer divers quantités. Dans la présente communication, on présente des mécanismes et des graphiques de contrainte, avec une comparaison entre les tassements observés et une prédiction d'essai, selon la méthode d'étude à résistance mobilisable (MSD).

Keywords: shallow foundations, saturated sand, centrifuge, settlement, strains, mechanisms

1 INTRODUCTION

All structures in contact with the ground require a foundation for support. Shallow foundations are frequently utilised for small-scale projects so their design is a common task for geotechnical engineers. Two issues are considered in the design of a shallow foundation – bearing capacity and settlement.

Research on shallow foundations has been performed for almost a century. Prandtl used the theory of plasticity to analyse the penetration of hard bodies into softer materials [1]. This research was extended by Terzaghi to apply to the bearing capacity of shallow foundations [2]. Many refinements have subsequently been added. Eurocode 7 provides a method for determining both the undrained and drained bearing resistance for current design engineers. A commonly used approach for vertical loading on frictional soils, with friction angle ϕ, is shown in Equation 1 with the given notation:

[1] Corresponding author.

$$q_f = s_q N_q \sigma'_{v0} + s_\gamma N_\gamma \frac{\gamma' B}{2} \quad (1)$$

- q_f is the bearing capacity
- s_q and s_γ are shape factors
- N_q and N_γ are bearing capacity factors
- σ'_{v0} is the effective overburden
- γ' is the effective unit weight, and
- B is the footing width, e.g. diameter

For circular footings with a rough base:

$$N_q = \tan^2(\pi/4 + \phi/2) e^{(\pi \tan\phi)} \quad (2)$$

$$N_\gamma = 2(N_q - 1)\tan\phi \quad (3)$$

$$s_q = 1 + \sin\phi \quad (4)$$

$$s_\gamma = 0.7 \quad (5)$$

2 SETTLEMENT

The settlement calculation is generally the most critical criterion for shallow foundation design, whether on clay [3] or on sand [4]. Despite this, relatively little effort has been expended to validate calculation methods for the settlement of shallow foundations.

Simplifications, such as assuming soil as an elastic medium, have been applied to the theory of three-dimensional consolidation of Biot [5], to produce current design methods.

There are two primary components of settlement – immediate (s_i) and consolidation (s_c). The secondary component of settlement (s_s) is longer-term and due to creep. The total settlement (s) is the summation in Equation 6.

$$s = s_i + s_c + s_s \quad (6)$$

2.1 Immediate Settlement

Loading of a saturated soil is immediately resisted by an increase in pore pressure. The resulting deformation is undrained and the soil consequently shears at constant volume. This settlement is often the most significant component of the total settlement.

To determine the immediate settlement undrained parameters, E_u and ν_u, are utilised. Soil, however, is highly non-linear even at very small strains, causing uncertainty, variability and error in design calculations. Osman and Bolton [6] use plasticity concepts, with strain hardening, and the non-linear stress-strain behaviour of soil, in the Mobilizable Strength Design (MSD) approach for the design of shallow foundations on clay. Pore pressure dissipation incites consolidation settlement.

2.2 Consolidation Settlement

The proportion of ultimate consolidation settlement due to 3-D pore pressure dissipation is expressed in a plot versus dimensionless time [7]. The magnitude is found as the difference between elastic calculations of 'drained' settlement (using E' and ν') and undrained settlement. Engineers, however, habitually measure the confined stiffness E'_0 from oedometer tests. The question arises again of the significance of the mismatch between available data and the assumptions of available theories.

2.3 Secondary Settlement

Research on creep has increased in recent years [8]. The magnitude of creep settlement is generally insignificant in comparison to both the undrained and consolidation settlements. It should not, however, be neglected for long term structures. Tests described in this paper were not performed for a sufficient duration to investigate creep.

3 CENTRIFUGE TESTING

The testing program was performed on the 10m diameter beam centrifuge in the Schofield Centre at Cambridge University. Experiments were performed in an aluminium package of dimensions 790mm × 200mm × 560mm deep. The front face of the package comprised a Perspex window. Semi-circular foundations were chosen to facilitate analysis in axial symmetry. Digital cameras were used to capture images at all stages of the footing loading. This allowed deforma-

tions to be calculated using Particle Image Velocimetry (PIV) [9].

One-dimensional actuators were developed to apply footing loads to the soil body. Compressed air acting through pneumatic cylinders, controlled by solenoids, was used to actuate movements. Problems encountered with an uneven sand surface required two different methods of applying a footing load to be utilized. In the initial loading method, the footing was bolted rigidly to the connecting rod of the pneumatic cylinder. This allowed load to be applied and increased through the application of compressed air to the top inlet of the pneumatic cylinder piston. An alternative loading method used the dead-weight of the footing – applying approximately 100kPa. A countersunk hole was drilled at the centre of gravity of the semi-circular footing. An M3 bolt through the footing attached it to a connecting rod which suspended the footing during spin-up and consolidation of the soil body by applying compressed air to the bottom inlet of the pneumatic cylinder. When ready, the air pressure was reduced steadily so that the footing dropped on to the soil surface loading it through its enhanced self-weight, as the M3 bolt fell clear. This is illustrated in Figure 1.

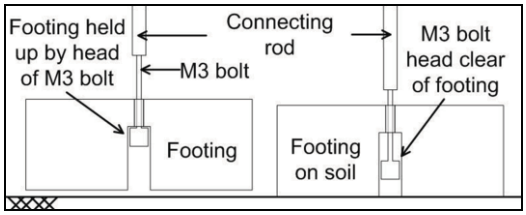

Figure 1. Dead-weight system used to hold the footing above the surface and to apply the load.

3.1 Instrumentation

Instrumentation was used to measure and verify various quantities in the experiments. Load cells were utilised to verify the load being applied by each footing. Pore Pressure Transducers (PPTs) were used to measure the static pore pressure and the excess induced upon footing loading. Finally, a MEMS Accelerometer was attached to the package to observe the appropriate testing g-level. The footings were tested at 100-g, measured at the surface of the soil.

3.2 Soil Body

Hostun sand was used as the soil body for this research. Grain distribution tests using Single Particle Optical Sizing (SPOS) analysis [10] produced a uniformity coefficient of U_c=1.6. Using the computer controlled sand pourer [11] a relative density I_D=49% (e=0.789) was achieved. To prevent scaling law discrepancies between model and prototype scales for consolidation and seepage velocity, the viscosity of the pore fluid was modified. The sand was saturated with methyl cellulose at a viscosity of 100cSt, thus 100 times that of water. Saturation was performed under vacuum by inundating the top of the model with the methyl cellulose solution. The vacuum was then turned off causing the model to saturate. The resulting prototype saturated unit weight was 18.9kN/m^3 giving a buoyant unit weight γ'=9.1kN/m^3. The soil body was allowed to consolidate in the centrifuge before the soil was loaded with the footings.

4 RESULTS AND DISCUSSION

4.1 Soil Surface

Rigid footings rigidly connected to a guide were not able to conform to uneven sand surfaces. Figure 2 portrays a footing immediately after loading occurred. It is evident that the footing load is applied on the right hand side, resulting in localized displacements. Subsequent load increases tended to spread the contact surface towards the left hand side. When constructing in hard soils and weak rocks the importance of leveling the surface before precast foundations are placed is apparent. Design calculations are performed assuming a level surface, but in-situ this may not occur, potentially resulting in differential settlements and possibly local structural failures.

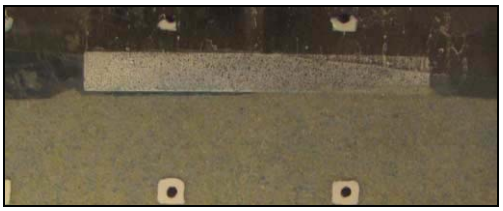

Figure 2. Uneven load distribution due to uneven surface

A PIV analysis was performed using digital images captured by a 14.7 Megapixel Canon Powershot G10 camera. Displacement mechanism and strain plots were produced based on the footing loading. These also assisted in demonstrating evenness of loading.

4.2 Observed Mechanism

A 50mm diameter dead-weight footing, 5m at prototype scale, applied a load of q=100kPa to the soil surface. The PIV analysis was performed on photographs taken before loading and about 3 seconds after. Given the high permeability of the sand the mechanism shown in Figure 3 portrays the fully drained mechanism (undrained penetration plus consolidation settlement).

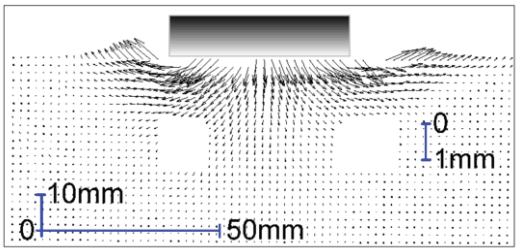

Figure 3. Mechanism observed for the 5m prototype scale footing.

A data interpolation script was written in Matlab R2009A to be utilized with the raw data. This ensures that data lost behind control markers or where there is a significant change in sand texture, is recognized and replaced. The result of the program running on the data in Figure 3 is shown in Figure 4.

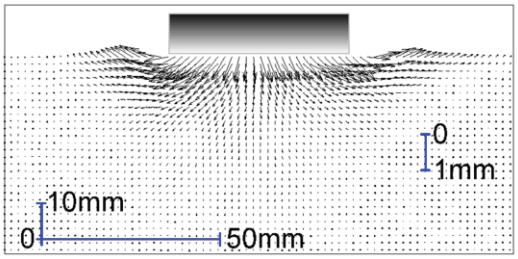

Figure 4. Interpolated mechanism for the 5m prototype scale footing.

Figure 4 confirms the vertical compression below the centre of the footing, with symmetric shear zones leading to heave adjacent to the footing edge. It is also evident that horizontal movement has occurred due to the relatively smooth interface between the footing and sand surface. Through PIV the observed footing movement was 1.3mm for the verified load of 100kPa, equivalent to 130mm at prototype scale. The area of influence due to footing loading is best observed on strain plots of the data.

4.3 Strain

Engineering shear strain, γ, and volumetric strain, ε_v, are determined by forming a triangle using any three known displacements. A mesh size of 1mm was used to perform the strain calculation. Figure 5 depicts the engineering shear strain (%) for the deformation mechanism shown in Figure 4. A threshold shear strain of 0.5% was set to remove noise incurred during PIV. Figure 6 portrays the volumetric strain (%) along the centerline of the footing with compression designated positive.

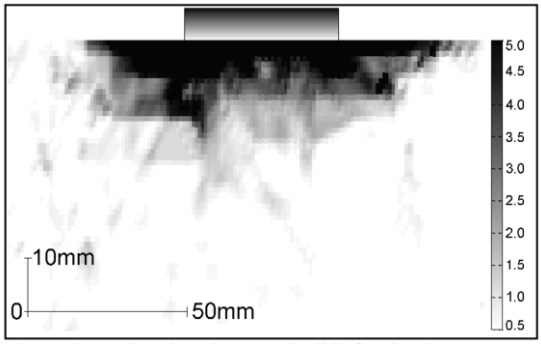

Figure 5. Engineering shear strain (%) for the 5m prototype scale footing.

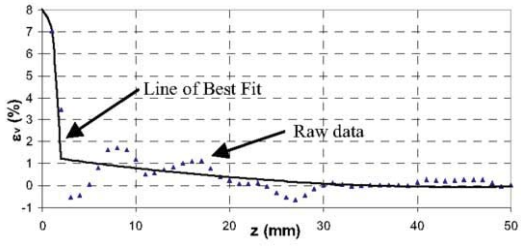

Figure 6. Volumetric strain (%) along the centerline of the 5m prototype scale footing (compression positive).

Integration of volumetric strains in Figure 6 produced a settlement due to volumetric strain of 0.28mm. Therefore, the settlement due to shear must be 1.02mm. From Figure 5 it can be seen that the depth affected by shearing is about 0.5B (one half of the footing diameter), whereas Figure 6 shows that volumetric compression continues to about a depth B=50mm.

4.4 Back Analysis

The equivalent linear shear strain, γ*, due to footing settlement is found using Atkinson's Method [12]:

$$\gamma^* = \frac{s}{2B} = 1.02\%$$

A hyperbolic shear stress-shear strain relationship was developed from a sand database and is shown in Equation 7 [13].

$$\frac{G^*}{G_0} = \frac{1}{1+\left(\frac{\gamma^*-\gamma_e}{\gamma_r}\right)^a} \tag{7}$$

The shear modulus, G_0, and characteristic strains, γ_r and γ_e, are functions of soil properties and the mean effective stress, p*. Expressions are given in Equations 8, 9 and 10 respectively. The curvature parameter, a, is given in Equation 11.

$$G_0 = \frac{57600}{(1+e)^3}\sqrt{p^*} \tag{8}$$

$$\gamma_r(\%) = 0.0001.U_c^{-0.3}.p^* + 0.08.e.I_D \tag{9}$$

$$\gamma_e(\%) = 0.0002 + 0.012.\gamma_r \tag{10}$$

$$a = U_c^{-0.075} \tag{11}$$

An expression for the settlement based on a circular punch is given in Equation 12 [14].

$$\frac{s}{B} = \frac{\pi}{8}\frac{(1-\nu)}{G^*}q \tag{12}$$

A value for the drained Poisson's ratio may be taken as ν=0.2. Using the centrifuge test results Equations 7-12 are solved, finding p*=19.5kPa.

In MSD analysis a representative location at a depth of 0.3B is used beneath a pad footing of diameter B – close to the centroid of the plastic deformation zone [6]. Figure 7 demonstrates the procedure for determining stresses before and during footing loading. A state of triaxial stress is assumed at these locations and hence a value for the mean effective stress, p', can also be determined using the portrayed formula.

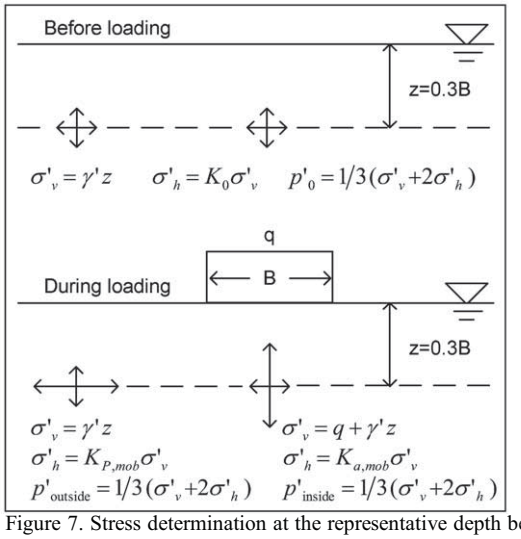

Figure 7. Stress determination at the representative depth before and after loading to find p'

Soil stresses before loading are determined using the at rest earth pressure coefficient, K_0, with the maximum friction angle, ϕ_{max}, calculated using Equation 13 and a critical state friction angle ϕ_{crit}=33° [15].

$$\phi_{\max} = \phi_{crit} + 3I_D(\ln(20000/p') - 1) \tag{13}$$

Utilizing the bearing capacity formulation in Equation 1, a mobilised friction angle can be determined for the applied load q=100kPa. Given there is no overburden at the footing base it is only an N_γ problem. The mobilised friction angle was determined to be 23°.

The representative depth [6] is z=1.5m at prototype scale. Results of calculations performed

at the representative depth before and after footing loading are shown in Table 1.

Table 1. Principal stresses and equivalent triaxial stress before and in the active and passive regions after loading

Parameter	Before Loading	Active Zone	Passive Zone
σ'_v	14kPa	114kPa	14kPa
K	0.33	0.44	2.28
σ'_h	4.5kPa	50kPa	31kPa
p'	8kPa	71kPa	19kPa

An operational value for p' should represent the average value of mean effective stress during loading. Thus, it is taken as a mean of the values before and after loading, $p'=1/2(p'_0 + p'_{loaded})$. The loaded value p'_{loaded} must represent an average value in space, and is taken as the geometric mean of p' below (inside), and surrounding (outside) the loaded footing. Therefore a possible calculated operational mean effective stress, $p'_{operational}$, could be:

$$p'_{operational} = \frac{1}{2}\left(p'_0 + \sqrt{p'_{inside} \cdot p'_{outside}}\right) = 22.5kPa$$

This operational mean stress is close to the ideal value p*=19.5kPa calculated earlier. This corresponds to a maximum shear modulus G_0=48000kPa and a settlement of 0.94mm. Both the settlement and mean effective stress correlate well between observed and calculated results.

5 CONCLUSION

Centrifuge experiments have been performed to observe deformation mechanisms beneath circular foundations on saturated Hostun sand. Experimental techniques and instrumentation have been described. Mechanisms, strains plots and a back analysis of settlement was performed with a small discrepancy between predicted and observed settlement of the foundation. Further research and analysis is scheduled with the aim of refining the settlement calculation procedure.

ACKNOWLEDGEMENT

This research was funded by a Poynton Scholarship awarded by the Cambridge Australia Trust and an Overseas Research Students (ORS) award.

REFERENCES

[1] L. Prandtl, Über die Eindringungsfestigkeit plastischer Baustoffe und die Festigkeit von Schneiden, *Zeitschrift für Angewandte Mathematik und Mechanik* **1** (1921), 15-20

[2] K. Terzaghi, *Theoretical Soil Mechanics*, John Wiley & Sons, New York, 1943

[3] G.G. Meyerhof, Shallow foundations, *Journal of the Soil Mechanics and Foundations Division* **91** (1965), 21–31

[4] E.E. De Beer, Bearing capacity and settlement of shallow foundations on sand, In *Bearing Capacity and Settlement of Foundations* (1965), 15–33

[5] M.A. Biot, General theory of three-dimensional consolidation, *Journal of Applied Physics* **12** (1941), 155–164

[6] A.S. Osman & M.D. Bolton, Simple plasticity-based prediction of the undrained settlement of shallow circular foundations on clay, *Geotechnique*, **55** (2005), 435-447

[7] J. R. Booker & J. C. Small, Finite layer analysis of viscoelastic layered materials, *International Journal for Numerical and Analytical Methods in Geomechanics* **10** (1986), 415–430

[8] J.-L. Briaud & R. Gibbens, Behavior of five large spread footings in sand, *Journal of Geotechnical and Geoenvironmental Engineering*, **125** (1999), 787-796

[9] D.J. White, W.A. Take & M.D. Bolton, Soil deformation measurement using particle image velocimetry (piv) and photogrammetry, *Geotechnique*, **53** (2003), 619-631

[10] D.J. White, PSD measurement using the single particle optical sizing (SPOS) method, *Geotechnique*, **53** (2003), 317-326

[11] Y. Zhao, K. Gafar, M.Z.E.B. Elshafie, A.D. Deeks, J.A. Knappet & S.P.G. Madabhushi, Calibration and use of a new automatic sand pourer. In C. Ng, L. Zhang & Y. Wang (Eds), *Physical Modelling in Geotechnics – 6th ICPMG '06,* Hong Kong, 265-270, Taylor and Francis Group, London

[12] J.H. Atkinson, Non-linear soil stiffness in routine design, *Geotechnique*, **50** (2000), 487-508

[13] S. Oztoprak & M.D. Bolton, Stiffness of sands through a laboratory test database, under review

[14] R.O. Davis & A.P.S. Selvadurai, *Elasticity and Geomechanics*, Cambridge University Press, Cambridge, 1996

[15] M.D. Bolton, The strength and dilatancy of sands, *Geotechnique*, **36** (1986), 65-78